I&EC research
Industrial & Engineering Chemistry Research

Article

pubs.acs.org/IECR

Nonlinear Model-Based Control of Thin-Film Drying for Continuous Pharmaceutical Manufacturing

Ali Mesbah, Ashlee N. Ford Versypt, Xiaoxiang Zhu, and Richard D. Braatz*

Department of Chemical Engineering, Massachusetts Institute of Technology, 77 Massachusetts Avenue, Cambridge, Massachusetts 02139, United States

ABSTRACT: This paper considers the model-based control of composition and thickness for a thin-film drying process used in the continuous manufacturing of pharmaceutical tablets. In this nonlinear distributed dynamical system, a drug formulation solution is coated onto a moving surface and then dried to form thin films of approximately 250 μm in thickness. A dynamic optimizer is designed that employs a first-principles process model to simulate the spatial distribution of solvent concentration in the film and the thin film shrinkage during drying. A critical parameter to describe the highly nonlinear dynamics of the thin-film drying is the mutual polymer−solvent diffusion coefficient, which strongly depends on solvent concentration and film temperature. Two optimal control problems are studied for set point tracking of solvent concentration and minimization of energy consumption in the dryer while satisfying various operational and product quality constraints. An unscented Kalman filter is designed to facilitate the output feedback implementation of the dynamic optimizer and to estimate unmeasured thin-film quality attributes such as the film thickness. The performance of the model-based controller is compared to that of a proportional integral controller in two simulation case studies. The nonlinear model-based control strategy has improved versatility and the potential to reduce production of off spec material.

1. INTRODUCTION

Continuous manufacturing is receiving increasing attention in the pharmaceutical industry to reduce time-to-market and production costs while enhancing product quality.[1,2] Traditionally, the batch mode of operation dominates the pharmaceutical industry. A shift from the batch mode of operation to the continuous mode, where raw materials are converted to the drug products in an integrated facility, offers opportunities to improve the overall flexibility, reliability, and efficiency of the production process.[3,4] In addition, continuous manufacturing facilitates the use of increased process understanding for online process control,[5] which can lead to consistently higher quality products as well as reduced waste generation and energy consumption.

The majority of pharmaceutical products are manufactured as solid tablets or capsules due to their low manufacturing cost, effective delivery of active pharmaceutical ingredients (APIs), designable disintegration profiles, and convenience of use.[6,7] However, tablets and capsules are composed of powders, which are difficult to handle and, more importantly, may lack API uniformity.[8] To address the manufacturing challenges of solid dosage forms, thin films that dissolve quickly have been developed as an oral drug delivery system in recent years.[9,10] Thin-film manufacturing is based on liquid solutions, which alleviate the solids-handling problems. Thin-film dosage forms are especially advantageous when the API cannot be dispersed well in a solid form or the solids handling reduces the API yield,[11] but the use of dissolving oral films is limited to APIs with fast metabolic uptake rates due to the rapid disintegration of thin films. The storage and transportation of thin films is also challenging because of their fragility and friability.[12]

A process of manufacturing pharmaceutical tablets from thin films has been developed at the Novartis−MIT Center for Continuous Manufacturing.[8] The continuous process for making thin-film tablets consists of four steps: preparation of the formulation solution, casting the solution as a thin layer that is dried to produce the thin film, folding of the dried thin film, and compaction of the folded thin film to form tablets. This process combines the merits of thin-film manufacturing in terms of minimal solids handling and fast drying times with the wider applicability of tablets for effective drug delivery.

This paper investigates advanced control of a continuous thin-film dryer that comprises the second step of the thin-film tablet manufacturing process. The film is coated onto a moving surface and dried in the thin-film dryer to remove solvents in the drug formulation solution. The mechanical characteristics and adhesion properties of thin films used in subsequent film folding, compaction, and extrusion operations heavily rely on the solvent composition in the film at the end of the drying process.[8] Controlling the solvent content and thickness of the thin film exiting the dryer is critical to the overall process of thin-film tablet formation.

In general, the control problem for film coating processes is separated into two control objectives: maintenance of uniform thickness along the length of the film, known in the literature as the *machine-direction control problem*, and maintenance of uniform properties across the width of the film, known as the *cross-directional control problem* (see the work of VanAntwerp et al.[13] and references therein). The control objective for the thin-film dryer studied in this paper is to regulate the film properties (composition and thickness) as the film moves through the

Special Issue: John Congalidis Memorial

Received: August 28, 2013
Revised: December 18, 2013
Accepted: December 18, 2013
Published: December 18, 2013

dx.doi.org/10.1021/ie402837c | *Ind. Eng. Chem. Res.* 2014, 53, 7447−7460

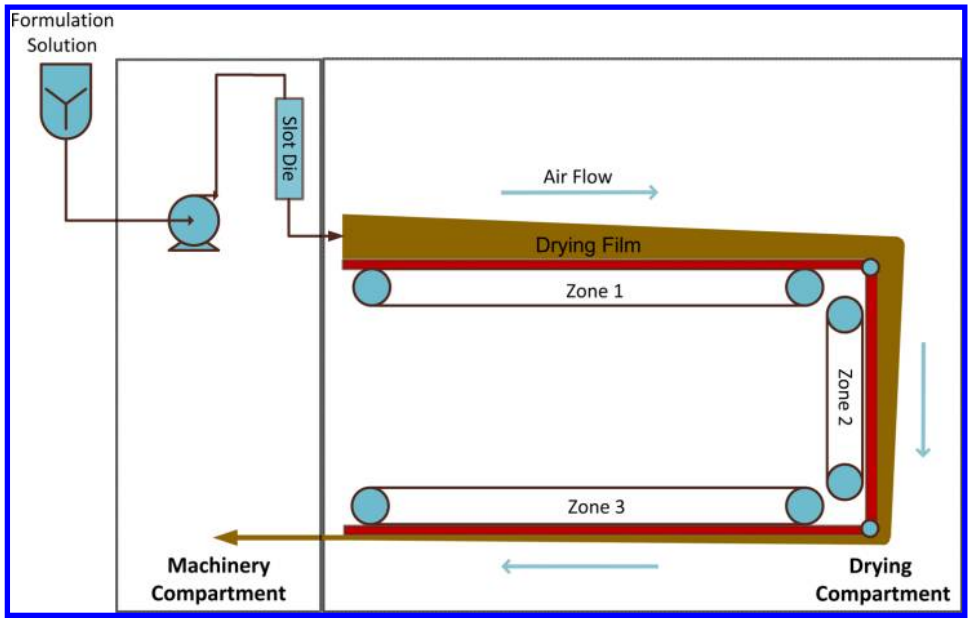

Figure 1. Schematic representation of the thin-film dryer.

dryer. The system dynamics in this machine-directional control problem are characterized by highly nonlinear dynamics in the composition evolution in the film, a characteristic that is shared by many other sheet and film processes.[14−17] In addition, due to their high costs, only a limited number of in situ sensors are usually used to measure the uniformity of film properties (especially film thickness) for online control applications.[18,19]

In this study, a nonlinear model-based controller is developed for optimal operation of the thin-film dryer. The use of model predictive control has long been considered for the control of sheet and film coating processes.[20−29] What distinguishes this work is the complex nonlinear distributed dynamics of composition evolution and the nonlinear film shrinkage throughout the drying process that necessitate the use of nonlinear state estimation and control techniques. Due to the change in film properties as the thin film moves through the dryer, there is a one-to-one correspondence between the drying time and the position of the film in the dryer. This correspondence implies that the control problem should be formulated with respect to a spatial domain and, therefore, the resulting operating policies correspond to the position of the thin film in the dryer at each time.

The cornerstone of the proposed nonlinear model-based controller is a dynamic optimizer that computes optimal operating policies in an online manner. In contrast to many model predictive control algorithms that employ a linear time-invariant model or updated linearizations of a nonlinear model so as to produce a quadratic program in the optimization step (e.g., see Landlust et al.[30] and Daraoui et al.[31]), dynamic optimization enables using a nonlinear process model for both simulating the process dynamics over a prediction horizon and computing the optimal control inputs.[32−40] An unscented Kalman filter[41−47] is designed to facilitate closed-loop implementation of the dynamic optimizer and to estimate unmeasured process variables (e.g., film thickness). The performance of the nonlinear model-based controller is compared to that of a proportional integral controller using two simulation case studies.

2. THIN-FILM DRYER

The thin-film dryer is partitioned into a compartment for machinery and a compartment for drying (see Figure 1 for a schematic representation). The film-guiding devices such as rollers and winder shafts that facilitate thin-film handling in the drying section are mounted in the machinery compartment. The formulation solution is pumped through a slot die in the machinery compartment and passes beneath a casting knife for uniform placement on a moving liner for transport through the drying compartment. The formulation solution is a polymeric aqueous solution that contains the API, plasticizer, and solvent. The cast fluid film enters the drying section through a slit at the top left of the compartment. The dryer consists of three drying zones arranged in a horizontal u-shaped configuration. In zone 1, air nozzles positioned in a row below the film blow hot air on a metal plate on which the film slides. Simultaneously, a fan blows hot air across the top side of the fluid film to remove the solvent loaded air. Approximately 85% of the solvent is evaporated at the end of zone 1.

After zone 1, the partially dried film is bent downward by a 90° guide and enters zone 2. The heating configuration of zone 2 is similar to that of zone 1, while its length is as half as long as zone 1. By the time the film passes through another 90° guide to enter zone 3, approximately 95% of the solvent has been removed. In zone 3, the thin film moves toward the machinery compartment with the surface of the film that is facing downward to be exposed to hot air flow.

Each drying zone has an individual fan and heater to independently control the temperature of the hot air blown into the zone. However, the rotational speed of the input and exhaust fans cannot be varied in the course of drying, which is a precaution to ensure that the solvent concentration in the exhaust air is always below the lower explosive limit. The film temperature and solvent concentration are measured at 18 equidistant points along the moving liner in the drying compartment.

dx.doi.org/10.1021/ie402837c | Ind. Eng. Chem. Res. 2014, 53, 7447−7460

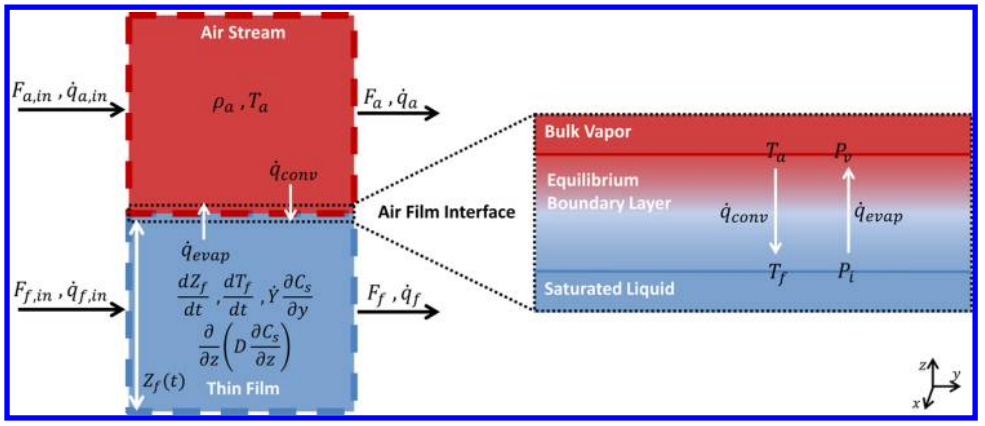

Figure 2. Transport processes between the air stream and thin film, and the process variables in the continuous thin-film drying.

3. DRYING MODEL

Drying of thin films involves simultaneous mass, heat, and momentum transport. A variety of models have been reported in the literature for drying of binary polymeric thin films in convection ovens.[48−50] Quantitative predictions of thin-film drying require accurate characterization of the falling-rate period of drying, which is a nonisothermal process often dominated by diffusion-limited behavior[51] and involves film shrinkage and the nonlinear dependence of the polymer−solvent mutual diffusion coefficient on temperature and concentration.

Figure 2 presents a schematic of the thin-film drying process. The evolution of the solvent concentration, C_s, and film temperature, T_f, governs the time-varying drying rate. The formulation solution is treated as a pseudobinary system where the components are lumped into two species: nonvolatile polymer and volatile solvent. The formulation solution is assumed to be ideal (i.e., no volume change occurs upon mixing).

The cast fluid film that enters the drier has a thickness $Z_f(t = 0) = L$ that decreases due to solvent evaporation as the film moves through the thin-film dryer along the y-direction. There is a one-to-one correspondence between the drying time and the position of the thin film along the dryer, implying that the residence time of the film in the dryer is equal to the total drying time. Concentration and temperature gradients are assumed to be negligible in the cross-directional (x) direction since the film is much wider than its thickness. In addition, the air convective resistance to heat transfer is greater than the conductive resistance in the film. Hence, it is a very accurate assumption that the thermal conduction in the z-direction is so rapid that the film temperature is uniform with respect to the z-direction. Potential complications associated with surface tension gradients and stress gradients in the film are neglected, as the surface of the thin film is very flat (minimum curvature effects) and the air provides negligible resistance to the film motion (i.e., the velocity gradient within the film with respect to the z-direction is negligible). The operating temperature of the dryer is above the glass transition temperature of the formulation solution and, therefore the heat capacity is a weak function of temperature throughout the drying process.

The mass balance of solvent in the film is described by the continuity equation

$$\frac{\partial C_s}{\partial t} + \dot{Y}\frac{\partial C_s}{\partial y} = \frac{\partial}{\partial z}\left(D(C_s, T_f)\frac{\partial C_s}{\partial z}\right) \tag{1}$$

where C_s is the weight fraction of solvent on a wet basis, t is the drying time, $\dot{Y}$ is the liner velocity in the y-direction, D is the polymer−solvent mutual diffusion coefficient, and T_f is the film temperature. The initial solvent weight fraction in the film is uniform

$$t = 0: \quad C_s(0, y, z) = C_{so} \tag{2}$$

where C_{so} is the solvent weight fraction in the formulation solution. The liner is assumed to be impenetrable to species in the film, which is a very accurate assumption, and, therefore, the zero-flux boundary condition is imposed at the film-liner interface

$$z = 0: \quad \frac{\partial C_s}{\partial z} = 0 \tag{3}$$

At the film−air interface, the solvent mass transfer from the film to the air determines the solvent flux

$$z = Z_f(t): \quad D(C_s, T_f)\frac{\partial C_s}{\partial z} + C_s\frac{dZ_f}{dt} = -\frac{k_m M_s}{\rho_s R}\left(\frac{P_i(T_f)}{T_f} - \frac{P_v(T_a)}{T_a}\right) \tag{4}$$

where Z_f is the time-varying film thickness, k_m is the mass transfer coefficient, ρ_s is the solvent density, M_s is the solvent molecular weight, R is the ideal gas constant, P_v is the solvent vapor pressure in the bulk air, T_a is the air temperature, and P_i is the equilibrium solvent partial pressure at the film−air interface. The boundary condition with respect to the convective flow of solvent in the downstream direction is given by

$$y = 0: \quad C_s(t, 0, z) = C_{so} \tag{5}$$

The continuity equation (eq 1) is coupled with the mass and energy conservation balances to describe the film thickness and temperature variations during drying. The mass balance for the film is

$$A\rho_f\frac{dZ_f}{dt} = F_{f,in} - \rho_f X\dot{Y}Z_f - \frac{k_m A M_s}{R}\left(\frac{P_i(T_f)}{T_f} - \frac{P_v(T_a)}{T_a}\right) \tag{6}$$

with initial condition

$$t = 0: \quad Z_f(0) = L \tag{7}$$

dx.doi.org/10.1021/ie402837c | Ind. Eng. Chem. Res. 2014, 53, 7447−7460

where A is the film surface area exposed to air, ρ_f is the film density, $F_{f,in}$ is the inlet formulation solution flow rate to the dryer, X is the width of the film, and L is the gap size of the casting knife.

The energy balance for the film includes heat transfer from the bulk air to the film through an effective heat transfer coefficient as well as evaporation heat of the solvent. The description of film temperature dynamics is simplified by the conduction of heat in the film being fast compared to convective heat transfer at the film−air interface. The energy balance is

$$A\rho_f c_p T_f \frac{dZ_f}{dt} + A\rho_f c_p Z_f \frac{dT_f}{dt} = h_{f,in}F_{f,in} - h_{f,out}\rho_f X\dot{Y}Z_f + Ak_c(T_a - T_f) - \frac{h_{fg}k_m AM_s}{R}\left(\frac{P_i(T_f)}{T_f} - \frac{P_v(T_a)}{T_a}\right) \quad (8)$$

with initial condition

$$t = 0: \quad T_f(0) = T_{f,in} \quad (9)$$

where c_p is the film heat capacity, $h_{f,in}$ is the enthalpy of the formulation solution, $h_{f,out}$ is the enthalpy of the film, k_c is the heat transfer coefficient, h_{fg} is the latent heat of vaporization of solvent, and $T_{f,in}$ is the temperature of the formulation solution.

In eqs 4, 6, and 8, the vapor pressure of solvent in the bulk air is considered to be constant throughout the drying process. In contrast, the solvent partial pressure at the film−air interface is computed on the basis of the solvent concentration and film temperature at the interface using the Flory−Huggins theory for phase equilibria.[52] The most critical model parameter is the polymer−solvent mutual diffusion coefficient, which is a strong function of solvent concentration and film temperature

$$D(C_s, T_f) = D_0\left(\frac{1 - \Phi_p(C_s)}{1 + \Phi_p(C_s)}\right)^{\gamma}\exp\left(\frac{-E_a}{RT_f}\right) \quad (10)$$

where D_0 is the reference mutual diffusion coefficient, Φ_p is the polymer volume fraction, γ is a constant, and E_a is the activation energy.

To facilitate the numerical solution of the model equations, the transformations

$$\psi = \frac{y - \dot{Y}t}{Y} \quad (11)$$

and

$$\eta = \frac{z}{Z_f(t)} \quad (12)$$

are applied to convert the fixed reference coordinate system into a moving reference coordinate system, where Y denotes the total length of the liner along the three drying zones. This transformation not only immobilizes the shrinking film−air interface with the variable, η, that always has values between 0 and 1 but also simplifies numerical solution of the continuity eq 1 by eliminating the term for the convective flow of solvent in the y-direction. The dimensionless forms of the model equations can be written as

$$\frac{\partial S}{\partial \tau} = \frac{1}{Z^{*2}}\frac{\partial}{\partial \eta}\left(\frac{D}{D_0}\frac{\partial S}{\partial \eta}\right) + \frac{\eta}{Z^*}\frac{dZ^*}{d\tau}\frac{\partial S}{\partial \eta} \quad (13)$$

$$\eta = 0: \quad \frac{\partial S}{\partial \eta} = 0$$

$$\eta = 1: \quad \frac{D}{D_0 Z^*}\frac{\partial S}{\partial \eta} + S\frac{dZ^*}{d\tau} = -\frac{Lk_m M_s}{D_0 C_{so}\rho_s R}\left(\frac{P_i(T_f)}{T_{f,in}T_f^*} - \frac{P_v(T_a)}{T_a}\right)$$

$$\frac{\rho_f D_0}{L}\frac{dZ^*}{d\tau} = -\frac{k_m M_s}{R}\left(\frac{P_i(T_f)}{T_{f,in}T_f^*} - \frac{P_v(T_a)}{T_a}\right) \quad (14)$$

$$\frac{\rho_f c_p Z^* T_{f,in} D_0}{L}\frac{dT_f^*}{d\tau} + \frac{\rho_f c_p T_{f,in}T_f^* D_0}{L}\frac{dZ^*}{d\tau} = k_c(T_a - T_{f,in}T_f^*) - \frac{h_{fg}k_m M_s}{R}\left(\frac{P_i(T_f)}{T_{f,in}T_f^*} - \frac{P_v(T_a)}{T_a}\right) \quad (15)$$

where the dimensionless variables are

$$\tau = \frac{D_0 t}{L^2}, \qquad S = \frac{C_s}{C_{so}}, \qquad Z^* = \frac{Z_f}{L}, \quad \text{and } T_f^* = \frac{T_f}{T_{f,in}} \quad (16)$$

and the initial conditions are

$$\tau = 0: \quad S(0, \psi, \eta) = 1, \qquad Z^*(0) = 1, \quad \text{and } T_f^*(0) = 1 \quad (17)$$

The derivation of eq 13 is given in the Appendix. The transformation of the reference coordinate system leads to elimination of the terms for the inlet and outlet streams in eqs 14 and 15. The physical properties of the polymer−solvent system and model parameters are listed in Table 1. The latent heat of vaporization h_{fg} (J/kg) is defined by[53]

$$h_{fg} = 2502535 - 2386(T_f - 273) \quad (18)$$

The nonlinear partial differential equation (eq 13) was solved by the finite volume method. The solution method entails discretization of the spatial variable domain (i.e., η) and the use of the linear upwind difference scheme to approximate derivatives with respect to the spatial variable.[54] The thin-film drying dynamics can be represented as a set of nonlinear ordinary differential equations of the form

$$\dot{\mathbf{X}} = \mathbf{F}(t, \mathbf{X}, \mathbf{Y}, \mathbf{U}, \Theta), \qquad \mathbf{X}(t_0) = \mathbf{X}_0, \quad \mathbf{Y} = \mathbf{H}(t, \mathbf{X}, \mathbf{Y}, \mathbf{U}, \Theta) \quad (19)$$

where $\mathbf{X}(t) = [S\ T_f^*\ Z^*]^T$ is the state vector comprised of the dimensionless solvent weight fraction distributed along the z-direction (one value for each discretization cell), the dimensionless film temperature, and the dimensionless film thickness; $\mathbf{Y}(t)$ is the vector of measured variables including solvent weight fraction in the film and film temperature; $\mathbf{U}(t)$ is the vector of system inputs (air temperature T_a); $\Theta = [k_m\ k_c\ \gamma\ \chi]^T$ is the vector of model parameters; $\mathbf{F}$ is an algebraic vector function of the dynamic state equations; and $\mathbf{H}$ is an algebraic vector function of the measurement equations. The next section describes the incorporation of the process model 19 into a nonlinear model-based control strategy for the thin-film dryer.

dx.doi.org/10.1021/ie402837c | Ind. Eng. Chem. Res. 2014, 53, 7447−7460

Table 1. Physical Properties and Model Parameters

variable	description	value	unit
A_1	drying area in zone 1	0.24	m^2
A_2	drying area in zone 2	0.12	m^2
A_3	drying area in zone 3	0.24	m^2
C_P	film heat capacity	2439.26	J/kg·K
C_{so}	initial solvent weight fraction in the film	0.77	kg solvent/kg film
D_0	reference polymer−solvent mutual diffusion coefficient	4.45×10^{-9}	m^2/s
E_a	activation energy	7.79×10^6	J/kmol
$F_{f,in}$	inlet solution flow rate to the dryer	3.34×10^{-7}	m^3/s
k_c	heat transfer coefficient	100	W/m^2·K
k_{m1}	mass transfer coefficient in zone 1	0.019	m/s
k_{m2}	mass transfer coefficient in zone 2	0.003	m/s
k_{m3}	mass transfer coefficient in zone 3	0.002	m/s
L	initial film thickness	0.002	m
M_s	solvent molecular weight	23.49	kg/kmol
P	operating pressure	101325	Pa
R	ideal gas constant	8314	J/kmol·K
$T_{f,in}$	initial film temperature	293.15	K
X	film width	0.2	m
$\dot{Y}$	liner velocity	8.33×10^{-4}	m/s
ρ_f	film density	969.93	kg/m^3
ρ_s	Solvent density	909.85	kg/m^3
χ	Flory−Huggins parameter	0.35	
γ	coefficient in eq 10	1.5	

4. NONLINEAR MODEL-BASED CONTROL APPROACH

Optimal operation of drying processes typically aims to reduce the drying time or energy consumption or to enhance the final product quality.[55−57] In the thin-film drying process, the mechanical characteristics and adhesion properties of the manufactured thin films are greatly affected by the course of the drying. Among the critical quality attributes of thin films are the film thickness and the solvent concentration in the film, which heavily influence the downstream processes of folding and compaction of the film to form tablets. In addition, the structural integrity of thin films should be preserved by avoiding defects such as bubbles or cracks, which can form due to unfavorable film temperatures.

The thin-film dryer has three manipulated variables—the hot air temperature in each of the three drying zones (See section 2). The liner velocity is not used as a manipulated variable in this study since it is to be employed for optimizing the production rate of the thin-film tablet manufacturing process train. The solvent weight fraction in the film and the film temperature measured at multiple points along the dryer are used for online process control.

The controller design problem is formulated in terms of an optimal control problem. The focus of this study is the startup of the thin-film dryer from the time the film first enters the dryer to when its leading tip first exits the dryer, which is the most challenging problem in the control of the dryer. As will be seen in the Results and Discussion section, the hot air temperatures in each of the three zones reach their optimal steady-state values by the end of this startup phase of the operation. The mathematical formulations enable steering the process into a desired operating regime (described by an objective function) while satisfying various operational and product quality constraints. Two control scenarios are considered:

- **Scenario 1**: The objective is to track a predetermined set point for the solvent concentration in the exit film while satisfying quality constraints on the thickness and structural integrity of thin films. The associated optimal control problem is

$$\min_{\mathbf{T}_a} \int_t^{t_d} (\bar{C}_s - C_{s,ref})^2 \, dt$$

subject to: eq (19)

$$303.15 \text{ K} \le T_{a,i} \le 348.15 \text{ K}, \quad i = 1, 2, 3$$

$$\left| \frac{dT_{a,i}}{dt} \right| \le 5.00 \text{ K}, \quad i = 1, 2, 3$$

$$Z_{f,exit} \le 4.25 \times 10^{-4} \text{ m}$$

$$P_b < P, \quad \forall\, t \in [0, t_d] \tag{20}$$

where $\boldsymbol{T}_a = [T_{a,1} \; T_{a,2} \; T_{a,3}]^T$ is the vector of manipulated variables consisting of hot air temperatures in the three drying zones, t_d is the total drying time (which was set to be large enough for the film to dry; its value would need to be increase if the liner velocity $\dot{Y}$ were reduced), $\bar{C}_s$ is the average solvent weight fraction over the film thickness at the exit of the machine, $C_{s,ref}$ is the admissible solvent weight fraction in the film at the exit of the machine, $Z_{f,exit}$ is the film thickness at the exit of the machine, P_b is the solvent partial pressure at the film−liner interface, and P is the operating pressure of the dryer. The inequality constraint $P_b < P$, which is enforced everywhere in the dryer, ensures that the solvent partial pressure at the film-liner interface remains below the operating pressure of the dryer at all times during drying to avoid bubble formation in the thin film.[58] The optimal control problem eq 20 also incorporates an input constraint on the hot air temperature in each drying zone. Note that the second inequality constraint in eq 20 enforces minimum and maximum temperature ramp rates to penalize excessively large control actions.

- **Scenario 2**: The objective is to minimize the energy consumption of the thin-film dryer while satisfying quality constraints on the solvent weight fraction in the film, the film thickness, and bubble formation. The optimal control problem is cast as

$$\min_{\mathbf{T}_a} Q_{air} = \sum_{i=1}^{3} A_a k_{c,a} (T_{a,i} - T_{a,in})$$

subject to: eq (19)

$$303.15 \text{ K} \le T_{a,i} \le 348.15 \text{ K}, \quad i = 1, 2, 3$$

$$\left| \frac{dT_{a,i}}{dt} \right| \le 5.00 \text{ K}, \quad i = 1, 2, 3$$

$$\bar{C}_s \le 0.05 \text{ kg solvent/kg film}$$

$$Z_{f,exit} \le 4.00 \times 10^{-4} \text{ m}$$

$$P_b < P, \quad \forall\, t \in [0, t_d] \tag{21}$$

where Q_{air} is the energy supplied to the heaters to heat the hot air streams, A_a is the heat exchange surface area of the heaters

dx.doi.org/10.1021/ie402837c | Ind. Eng. Chem. Res. 2014, 53, 7447−7460

used to heat the inlet air, $k_{c,a}$ is the heat transfer coefficient of air, and $T_{a,in}$ is the inlet air temperature. Like eq 20, the inequality constraint $P_b < P$ is enforced along the dryer.

To circumvent performance degradation of the optimal operating policies due to model imperfections and process disturbances, the underlying model in the optimal control problem should be continually updated using process measurements. Figure 3 shows the inclusion of the estimator in the

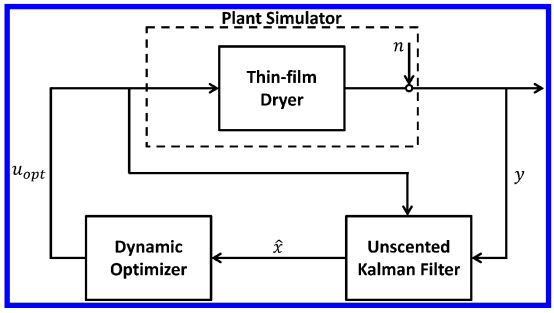

Figure 3. Nonlinear model-based control approach applied to the thin-film dryer.

output feedback control structure adopted for real-time control of the thin-film dryer. As in the model predictive control of batch processes,[32,59−61] the optimal control problem given by either eq 20 or 21 is solved online in a shrinking horizon mode. The optimal input sequences are recomputed at each sampling time instant, when new process measurements become available, by solving the optimal control problem over a finite time frame— the prediction horizon. The prediction horizon shrinks as the thin film moves toward the exit of the dryer. As in traditional receding horizon control, only the first computed time instance of each optimal input sequence is applied to the process at each sampling time instant.

The output feedback structure in Figure 3 necessitates recursive initialization of the dynamic optimizer at each sampling time instant. This initialization is performed by an unscented Kalman filter (UKF)[41,42] that uses the process model, along with online measurements, to construct the profile of state variables. Unscented Kalman filtering is a derivative-free state estimation technique that avoids linearization of the process model through an unscented transformation, while being computationally inexpensive (see the work of Mesbah et al.[47] for further discussion and a numerical study that compares UKF with other state estimators). Recursive initialization of the dynamic optimizer in the feedback control structure compensates for model imperfections and process disturbances to a large extent. In addition, the state estimator enables estimation of process variables such as film thickness that cannot be measured online due to technological or economic limitations.

To solve the optimal control problem, the infinite-dimensional problem is converted into a finite-dimensional nonlinear program (NLP) using the direct single shooting optimization strategy.[62] The single shooting optimizer is implemented in MATLAB where the model equations (a set of highly nonlinear stiff ordinary differential equations) and the NLP are sequentially solved by *ode15s* and *fmincon*, respectively. In the UKF, the deterministically chosen sigma points are selected symmetrically around the a priori state vector with a distance of the square root of the covariance.[63] As shown in Figure 3, the control strategy is applied to a plant simulator of the dynamics of the thin-film dryer, which exploits a nonlinear process model identical to that used in the UKF and the dynamic optimizer. The process measurements are corrupted by random noise sequences having normal distributions. The measurements are sampled every 200 s.

The performance of the model-based control strategy is evaluated with respect to a classical control strategy consisting of a proportional integral (PI) controller to regulate the concentration of solvent remaining in the film. The parameters of the PI controller are determined by characterizing the open-loop system dynamics and applying the internal model control (IMC) tuning rules for a first-order-plus-dead-time system.[64] In the classical control approach, a soft sensor is designed for process monitoring to estimate the unmeasured film thickness in the absence of accurate online measurement sensor. The soft sensor consists of the nonlinear process model (eq 19), which is solved in parallel with the real process by using the same input **U** as that applied to the process. The soft sensor is initialized recursively at regular time intervals when measurements become available. Like the UKF, the soft sensor

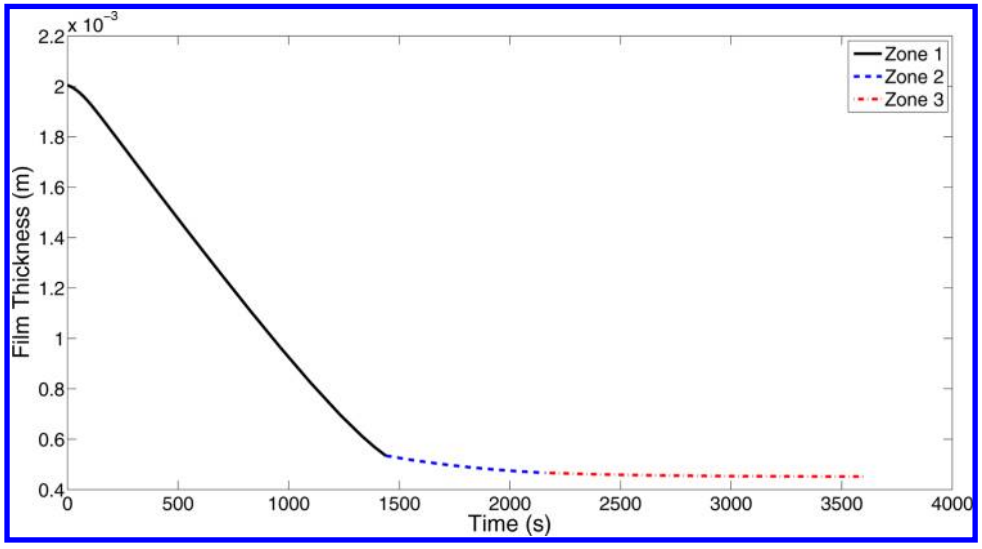

Figure 4. Film thickness profile in the thin-film dryer.

dx.doi.org/10.1021/ie402837c | Ind. Eng. Chem. Res. 2014, 53, 7447−7460

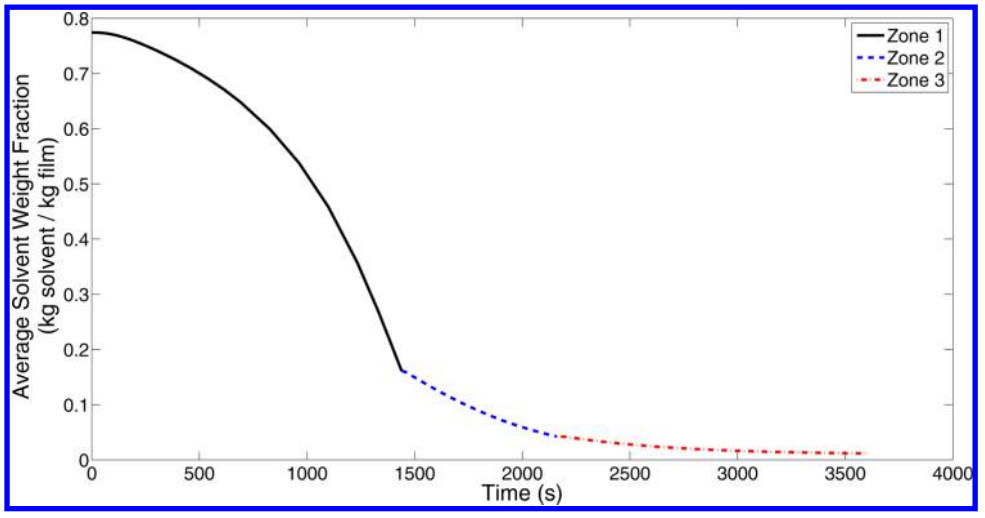

Figure 5. Average solvent weight fraction profile in the thin-film dryer.

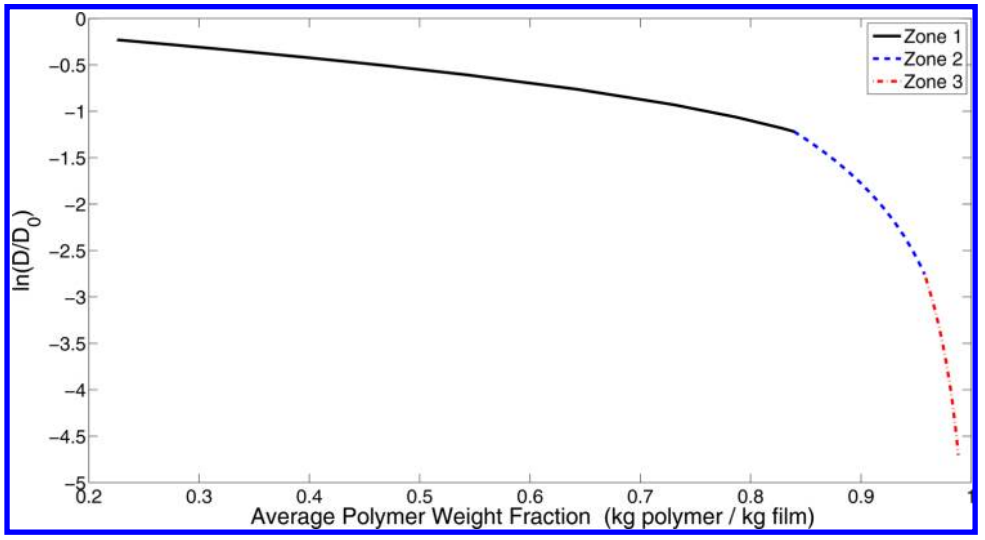

Figure 6. Variation of the mutual polymer−solvent diffusion coefficient in the thin-film dryer.

estimates the unmeasured film thickness by using the film temperature and solvent concentration measurements, which are obtained at equidistant points along the moving liner in the drying compartment (see section 2).

5. RESULTS AND DISCUSSION

5.1. Process Dynamics. This section explores the open-loop dynamics of the thin-film dryer. The manipulated variables— the hot air temperatures in the three drying zones—are initially set to 333.15 K (the initial and operating conditions are given in Table 1). Figure 4 shows the evolution of the film thickness in the course of the drying. The thickness of the fluid film is reduced significantly in zone 1 and to a lesser extent in zones 2 and 3. These reductions are associated with rapid solvent evaporation in zone 1, which leads to a steep decrease in the average solvent weight fraction in the film (see Figure 5).

Initially, the thin-film drying is limited primarily by external heat and mass transfer at the film−air interface, resulting in fast solvent removal from the film in zone 1. As the film moves through zones 2 and 3, molecular diffusion of the solvent in the drying thin film gradually limits mass transport, hindering the solvent removal. The variation of the mutual polymer−solvent diffusion coefficient as a function of the average polymer weight fraction over the three drying zones is depicted in Figure 6. The mutual diffusion coefficient, which is strongly dependent on the solvent concentration in the film, reduces by approximately 5 orders of magnitude during the drying. The steep decrease in the solvent diffusivity greatly reduces the solvent removal rate from the thin film in zone 3 (see Figure 5). Figure 5 indicates that 79.3%, 94.5%, and 98.6% of the initial amount of solvent in the formulation solution is removed at the end of zones 1, 2, and 3, respectively.

Figure 7 shows the evolution of the solvent weight fraction in the three drying zones. The solvent content of the fluid film decreases rapidly at the beginning of the drying in zone 1 due to the convective solvent removal from the film (see Figure 7a). The spatial gradient in the concentration in the film is relatively small during the initial part of the drying. However, as the drying proceeds, significant concentration gradients develop within the film, particularly in zone 3 (see Figure 7c), due to the strong diffusional resistance that severely slows the solvent removal rate. Large enough concentration gradients indicate skin formation on the surface of the thin film, which is a common phenomenon in the drying of single-layer polymer films.[65]

dx.doi.org/10.1021/ie402837c | Ind. Eng. Chem. Res. 2014, 53, 7447−7460

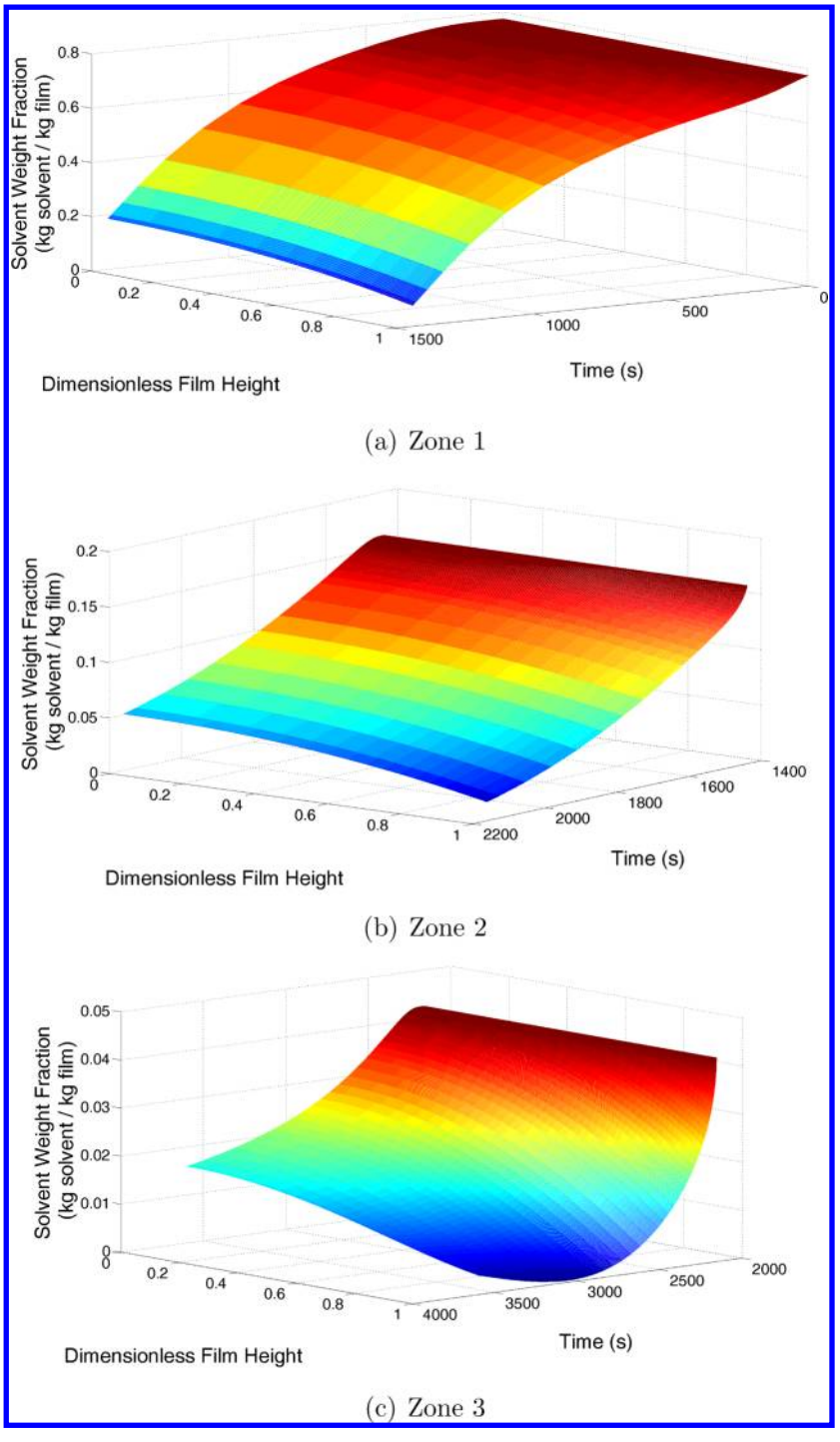

Figure 7. Evolution of the solvent weight fraction in the thin-film dryer.

Figure 8 shows the evolution of the film temperature, which exhibits first-order dynamics in each of the drying zones and asymptotically increases to the hot air temperature in zone 3 as the cooling effect associated with vaporization of the solvent gradually diminishes due to lower solvent evaporation rates. Figure 8 indicates that the film temperature dynamics are significantly faster than the dynamics of the solvent concentration variations in the film (see Figure 5), which is a result of both the thermal diffusion in the thin film being much larger than the molecular diffusion ($30 <$ Lewis number $< 7 \times 10^5$) and the thermal convection dynamics being a few orders of magnitude faster than the mass convection dynamics ($2 \times 10^3 < k_c/k_m < 5 \times 10^4$).

5.2. State Estimation. An unscented Kalman filter and a soft sensor are employed in the optimal and classical control strategies, respectively, to estimate the unmeasured film thickness using online measurements of solvent concentration and film temperature. Figure 9 depicts the open-loop estimation profiles produced by the UKF and soft sensor when the temperature of hot air in the three drying zones was set to 343.15 K. The soft sensor produced a noisy estimate of the solvent concentration whereas the UKF provided effective suppression of the effects of measurement noise (see Figure

dx.doi.org/10.1021/ie402837c | Ind. Eng. Chem. Res. 2014, 53, 7447−7460

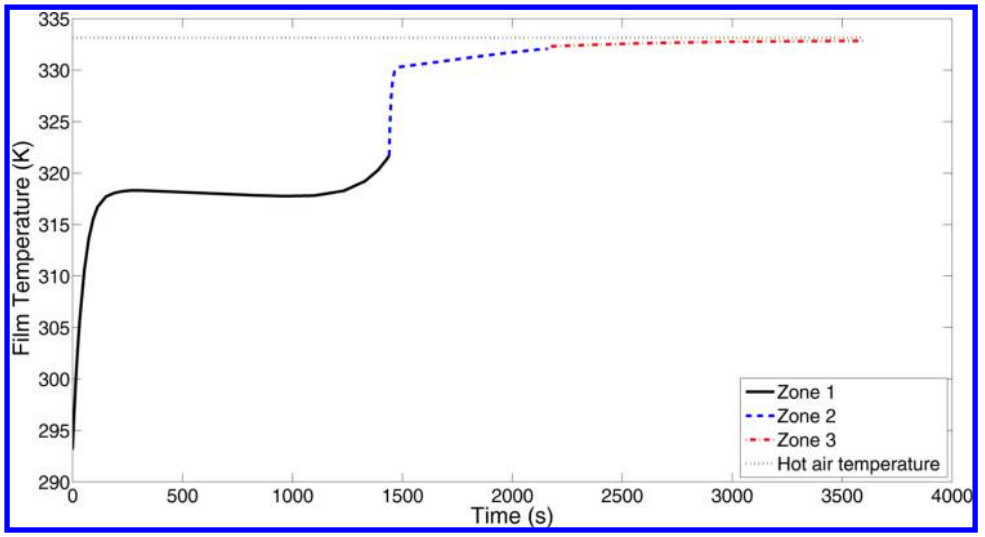

Figure 8. Film temperature profile in the thin-film dryer.

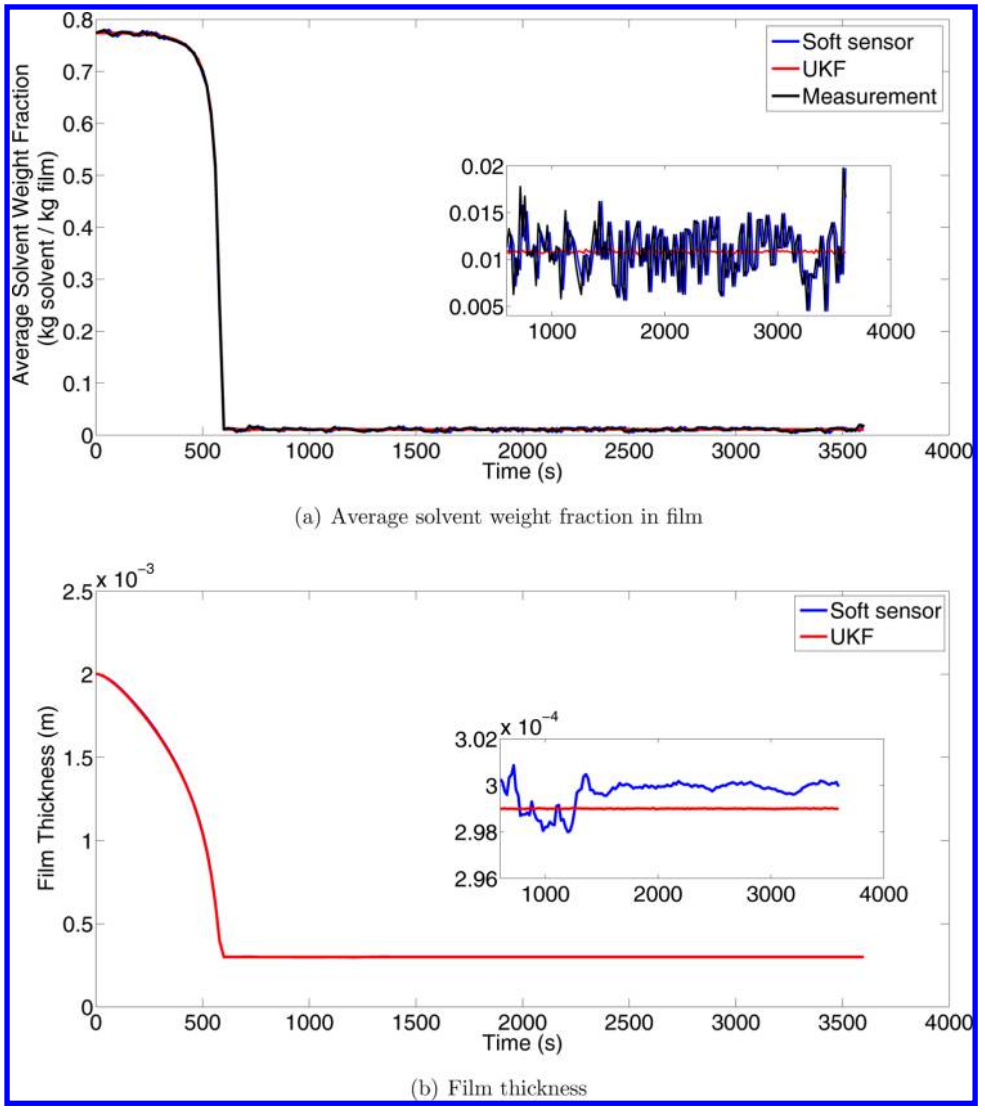

Figure 9. Comparison of estimated states obtained from the unscented Kalman filter and the soft sensor.

9a). This observation is not surprising, since the UKF is a stochastic estimation framework whereas the soft sensor is deterministic, which merely uses the nonlinear process model to simulate the evolution of system dynamics based on the

dx.doi.org/10.1021/ie402837c | Ind. Eng. Chem. Res. 2014, 53, 7447−7460

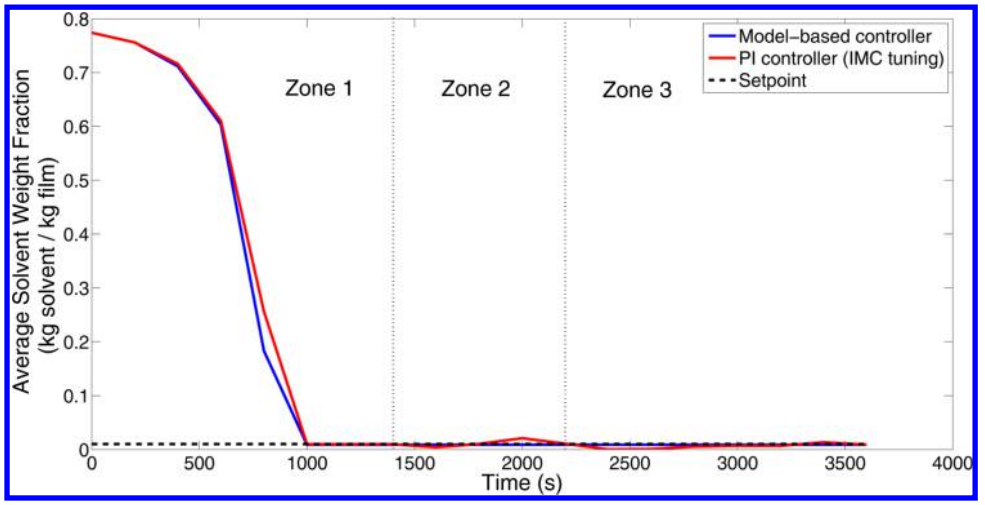

Figure 10. Average solvent weight fraction profile in scenario 1.

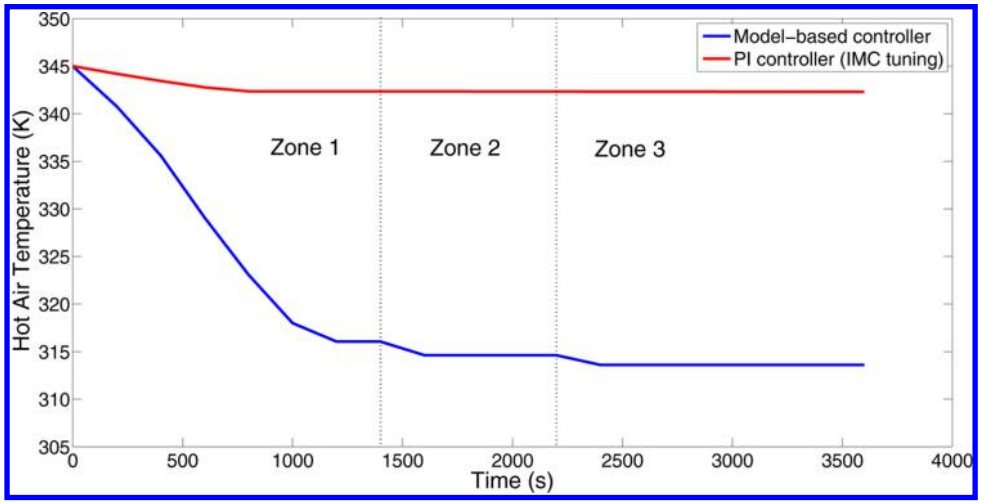

Figure 11. Hot air temperature profile in scenario 1, showing the temperature to which the film is exposed as it moves through the machine. For the model-based controller, the hot air temperature dropped sharply over time as the film moved through zone 1, then was slowly reduced over time to a new value while the film moved through zone 2, and then similarly for zone 3.

current state of the process. The UKF also led to much smoother film thickness estimates throughout the thin-film drying (see Figure 9b). Note that the PI controller directly used the online solvent concentration measurements rather than incorporating either the UKF or soft sensor.

5.3. Process Control. *5.3.1. Scenario 1.* Figure 10 shows the evolution of the average solvent weight fraction in Scenario 1, where the model-based control strategy is applied to follow the set point $C_{s,ref}$ = 0.01 kg solvent/kg film while fulfilling the quality constraints of the thin film (see eq 20). After significant removal of the solvent from the film in zone 1, the model-based controller closely tracks its predetermined set point in the average solvent weight fraction in zones 2 and 3. The PI controller produced some fluctuation and poorer tracking of the average solvent weight fraction in zones 2 and 3 (see Figure 10), but the film exiting the dryer, which is what is important in terms of product quality, was close to the set point for both control systems.

Figure 11 shows the evolution of the manipulated variable, hot air temperature, for the two control systems. The manipulated variables are qualitatively different. For the PI controller, the manipulated variable reduces over half of zone 1 and then remains constant for the rest of drying. For the model-based controller, the hot air temperature drops sharply in zone 1 to enforce set point tracking. When the film enters zone 2, the hot air temperature of the model-based controller reduces merely for approximately 2 K to facilitate close set point tracking by minimizing the evaporation of solvent molecules that can still reach the film−air interface. The manipulated variable remains almost constant in zone 3, as the solvent weight fraction is at its set point and further evaporation of the solvent remaining in the film is heavily hindered by diffusion. For the model-based controller, the hot air temperature in zone 1 reaches its optimal steady-state value after 1200 s, whereas the hot air temperature reaches its optimal steady-state value in about 200 s after the film first reaches zone 2, and similarly for zone 3. The film exiting the dryer has a much higher temperature for the PI controller than the model-based controller (Figure 11).

Two additional quality attributes of the thin film—the film thickness and the solvent partial pressure at the film−liner interface—are shown in Figure 12. For both control strategies, the thickness of the film exiting the dryer is within the admissible range for scenario 1, while the solvent partial

dx.doi.org/10.1021/ie402837c | Ind. Eng. Chem. Res. 2014, 53, 7447−7460

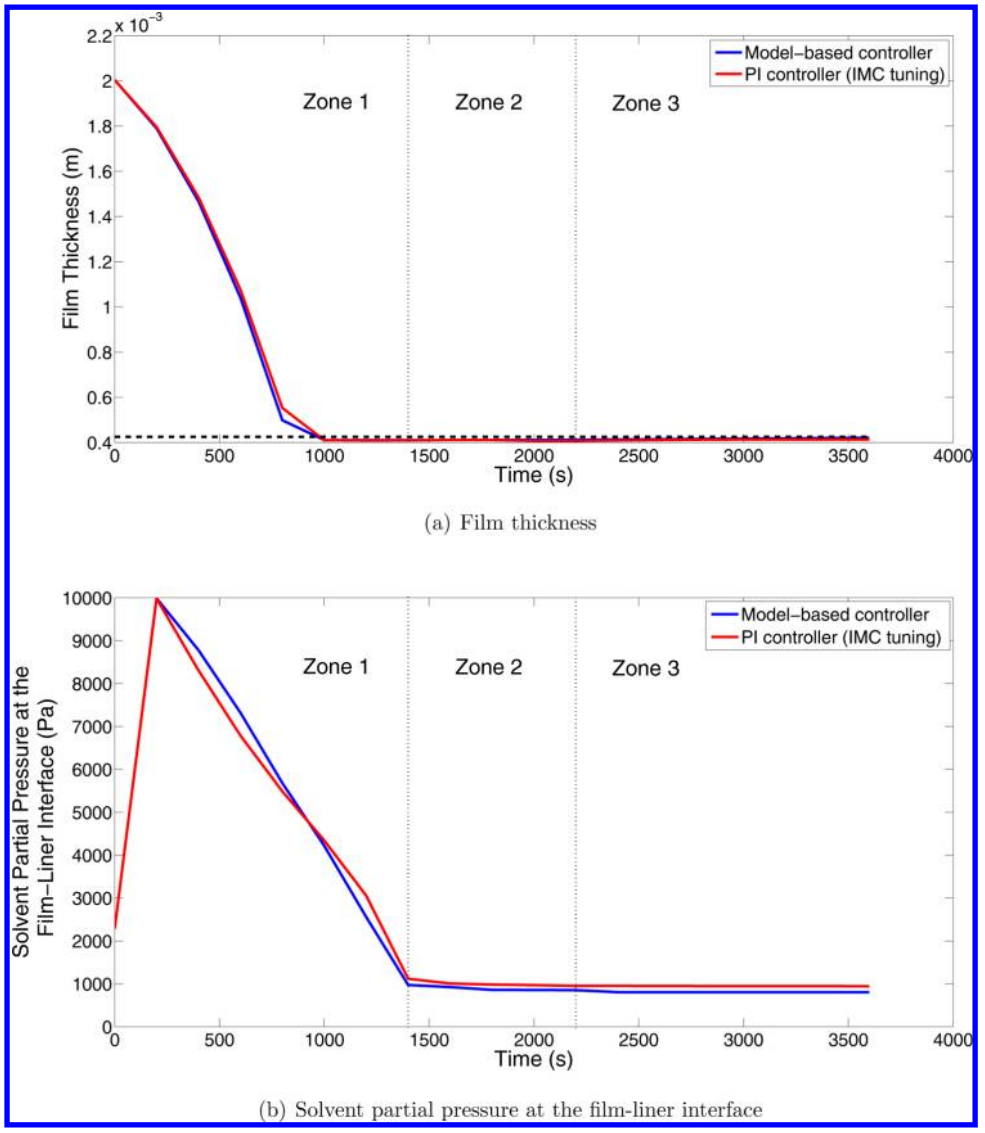

Figure 12. Quality attributes of the thin film in scenario 1.

pressure at the bottom of the film is consistently below the operating pressure of the dryer, avoiding the formation of bubbles in the film.

5.3.2. Scenario 2. Figure 13 shows quality attributes of the thin film in scenario 2, where the energy consumption of the dryer is minimized. This optimal control problem includes an additional constraint to attain a desired solvent composition in the exiting film (see eq 21). The set point of the PI controller is defined in terms of the maximum admissible solvent concentration ($C_{s,ref}$ = 0.05 kg solvent/kg film). Figure 13 suggests that the solvent mass fraction and thickness of the thin film are within their admissible specification ranges, whereas in the PI controller case the film thickness specification is not met. The optimal operating policy results in approximately 3.9% lower consumption of the total energy used to heat the hot air stream in the three drying zones, compared to the classical control strategy.

6. CONCLUSIONS

A first-principles model was developed for a thin-film dryer that comprises a key step in the continuous manufacturing of pharmaceutical tablets from thin films. The process model describes the dynamic evolution of the primary quality attributes of the thin films, namely, the film thickness and solvent composition. Characterizing the mutual polymer−solvent diffusion coefficient, which strongly depends on solvent concentration and film temperature, is central to describing the highly nonlinear dynamics of the thin-film drying. The focus was primarily on startup operations, with the objective being for the product film to satisfy all product quality specifications during startup, so that downstream operations would immediately have acceptable material.

The process model was used to design a nonlinear model-based controller for real-time control of the thin-film dryer. An unscented Kalman filter was designed to facilitate the implementation of the controller and to estimate the unmeasured film thickness. The performance of the model-based controller was compared to a PI controller in two control scenarios. The model-based control system provided significantly improved performance in both scenarios, with the PI controller barely meeting specifications on the product film for one scenario and not satisfying specifications for another scenario. It was also shown that the model-based controller

dx.doi.org/10.1021/ie402837c | Ind. Eng. Chem. Res. 2014, 53, 7447−7460

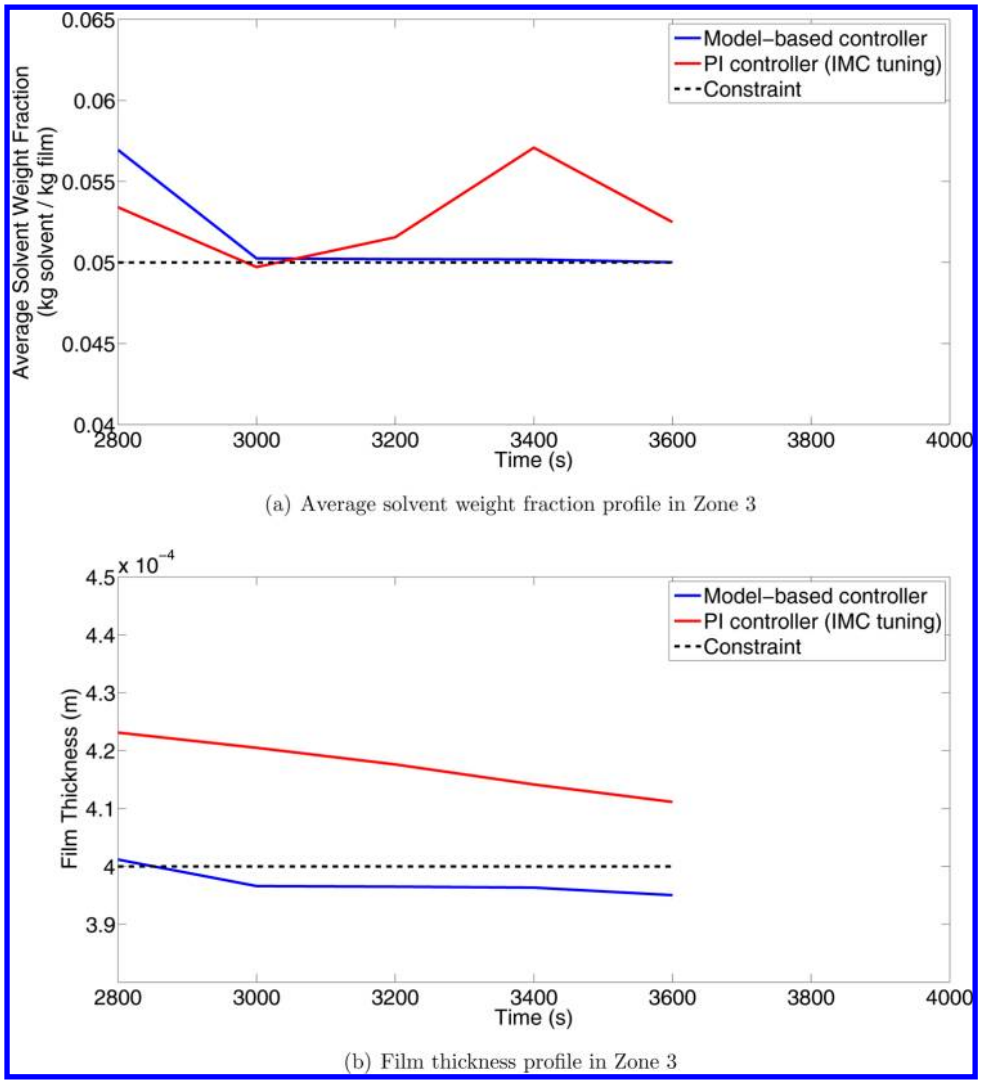

Figure 13. Quality attributes of the thin film in scenario 2.

resulted in a modest improvement in the energy efficiency of the thin-film dryer.

The comparison of the closed-loop performance of the two control strategies was under conditions that match the particular formulations and operations being investigated at the Novartis−MIT Center for Continuous Manufacturing. The nonlinear model-based control strategy has the potential to reduce off spec material (as seen in scenario 2) and has improved versatility, which should be useful when handling new pharmaceutical formulations and in later studies when the drying process is connected to a downstream process for continuous film folding and compaction.

APPENDIX

To transform eq 1 into its dimensionless form (eq 13), $\partial C_s/\partial t$ is written as

$$\frac{\partial C_s}{\partial t} = C_{so}\left(\frac{\partial S}{\partial \tau}\frac{\partial \tau}{\partial t} + \frac{\partial S}{\partial \psi}\frac{\partial \psi}{\partial t} + \frac{\partial S}{\partial \eta}\frac{\partial \eta}{\partial t}\right) \tag{22}$$

where

$$\frac{\partial \psi}{\partial t} = -\frac{\dot{Y}}{Y} \tag{23}$$

$$\begin{aligned}\frac{\partial \eta}{\partial t} &= \frac{-z\frac{\partial Z_f}{\partial t}}{Z_f^{\,2}(t)} \\ &= -\eta\frac{1}{Z_f(t)}\frac{\partial Z_f}{\partial t} \\ &= \frac{-\eta}{Z^*}\frac{\partial Z^*}{\partial t} \\ &= \frac{-\eta D_0}{Z^* L^2}\frac{\partial Z^*}{\partial \tau}\end{aligned} \tag{24}$$

Insertion of eqs 23 and 24 into eq 22 results in

$$\frac{\partial C_s}{\partial t} = C_{so}\frac{D_0}{L^2}\frac{\partial S}{\partial \tau} - C_{so}\frac{\dot{Y}}{Y}\frac{\partial S}{\partial \psi} - C_{so}\frac{\eta D_0}{Z^* L^2}\frac{\partial Z^*}{\partial \tau}\frac{\partial S}{\partial \eta} \tag{25}$$

The spatial derivative terms are defined by

$$\frac{\partial C_s}{\partial y} = C_{so}\frac{\partial S}{\partial \psi}\frac{\partial \psi}{\partial y} = C_{so}\frac{1}{Y}\frac{\partial S}{\partial \psi} \tag{26}$$

$$\frac{\partial C_s}{\partial z} = C_{so}\frac{\partial S}{\partial \eta}\frac{\partial \eta}{\partial z} = C_{so}\frac{1}{Z(t)}\frac{\partial S}{\partial \eta} \tag{27}$$

dx.doi.org/10.1021/ie402837c | Ind. Eng. Chem. Res. 2014, 53, 7447−7460

Substitution of eqs 25−27 into eq 1 leads to eq 13.

AUTHOR INFORMATION

Corresponding Author

*E-mail: braatz@mit.edu.

Notes

The authors declare no competing financial interest.

ACKNOWLEDGMENTS

Novartis Pharma AG is acknowledged for financial support.

REFERENCES

(1) Leuenberger, H. New Trends in the Production of Pharmaceutical Granules: Batch Versus Continuous Processing. *Eur. J. Pharm. Biopharm.* **2001**, *52*, 289−296.

(2) McKenzie, P.; Kiang, S.; Tom, J.; Rubin, A. E.; Futran, M. Can Pharmaceutical Process Development Become High Tech? *AIChE J.* **2006**, *52*, 3990−3994.

(3) Plumb, K. Continuous Processing in the Pharmaceutical Industry: Changing the Mind Set. *Chem. Eng. Res. Des.* **2005**, *83*, 730−738.

(4) Schaber, S. D.; Gerogiorgis, D. I.; Ramachandran, R.; Evans, J. M. B.; Barton, P. I.; Trout, B. L. Economic Analysis of Integrated Continuous and Batch Pharmaceutical Manufacturing: A Case Study. *Ind. Eng. Chem. Res.* **2011**, *50*, 10083−10092.

(5) Kockmann, N.; Gottsponer, M.; Zimmermann, B.; Roberge, D. M. Enabling Continuous Flow Chemistry in Microstructured Devices for Pharmaceutical and Fine Chemical Production. *Chem.—Eur. J.* **2008**, *14*, 7470−7477.

(6) Blanco, M.; Alcalá, M. Content Uniformity and Tablet Hardness Testing of Intact Pharmaceutical Tablets by Near Infrared Spectroscopy: A Contribution to Process Analytical Technologies. *Anal. Chim. Acta* **2006**, *557*, 353−359.

(7) Yu, L. Pharmaceutical Quality by Design: Product and Process Development, Understanding, and Control. *Pharm. Res.* **2008**, *25*, 781−791.

(8) Du, Y.; Luna, L. E.; Chadwick, K.; Kim, K. T.; Xi, L.; Myerson, A. S.; Trout, B. L. A Novel Thin Film-Based Pharmaceutical Tablet Manufacturing Process: Formulation, Processing, and Properties. 2013, submitted for publication.

(9) Dinge, A.; Nagarsenker, M. Formulation and Evaluation of Fast Dissolving Films for Delivery of Triclosan to the Oral Cavity. *AAPS PharmSciTech* **2008**, *9*, 349−356.

(10) Hirani, J. J.; Rathod, D. A.; Vadalia, K. R. Orally Disintegrating Tablets: A Review. *Trop. J. Pharm. Res.* **2009**, *8*, 161−172.

(11) Kunte, S.; Tandale, P. Fast Dissolving Strips: A Novel Approach for the Delivery of Verapamil. *J. Pharm. BioAllied Sci.* **2010**, *2*, 325−328.

(12) Arya, A.; Chandra, A.; Sharma, V.; Pathak, K. Fast Dissolving Oral Films: An Innovative Drug Delivery System and Dosage Form. *Int. J. ChemTech Res.* **2010**, *2*, 576−583.

(13) VanAntwerp, J. G.; Featherstone, A. P.; Braatz, R. D.; Ogunnaike, B. A. Cross-directional Control of Sheet and Film Processes. *Automatica* **2007**, *43*, 191−211.

(14) Lindeborg, C. A Simulation Study of the Moisture Cross-directional Control Problem. In *Instrumentation and Automation in the Paper, Rubber, Plastics, and Polymerization Industries*; Kaya, A., Williams, T. J., Eds.; Pergamon Press: Oxford, U.K., 1986; pp 59−64.

(15) Kjaer, A. P.; Wellstead, P. E.; Heath, W. P. On-Line Sensing of Paper Machine Wet-End Properties: Dry Line Detector. *IEEE Trans. Control Sys. Technol.* **1997**, *5*, 571−585.

(16) Vyse, R.; Hagart-Alexander, C.; Heaven, M.; Steele, T.; Chase, L.; Goss, J.; Preston, J. High Speed Full Cross Direction Profile Measurements and Control for the Paper Machine Wet End. *Proceedings of the 52nd APPITA Annual General Conference*, Carlton, Australia, May 11−14, 1998; pp 435−442.

(17) Poirier, D.; Vyse, R.; Hagart-Alexander, C.; Heaven, M.; Ghofraniha, J. New Trends in CD Weight Control for Multi-Ply Applications. *Pap. Technol. Ind.* **1999**, *40*, 41−50.

(18) Toensmeier, P. A. Sensor Scans 1000 Sites at 10 in./sec. *Mod. Plast.* **1991**, *68*, 35−37.

(19) Shelley, P. H.; Booksh, K. S.; Burgess, L. W.; Kowalski, B. R. Polymer Film Thickness Determination with a High Precision Scanning Reflectometer. *Appl. Spectrosc.* **1996**, *50*, 119−125.

(20) Bergh, L. G.; Macgregor, J. F. Spatial Control of Sheet and Film Forming Processes. *Can. J. Chem. Eng.* **1987**, *65*, 148−155.

(21) Braatz, R. D.; Tyler, M. L.; Morari, M.; Pranckh, F. R.; Sartor, L. Identification and Cross-Directional Control of Coating Processes. *AIChE J.* **1992**, *38*, 1329−1339.

(22) Halouskova, A.; Karny, M.; Nagy, I. Adaptive Cross-directional Control of Paper Basis Weight. *Automatica* **1993**, *29*, 425−429.

(23) Tyler, M. L.; Morari, M. Estimation of Cross-Directional Properties: Scanning vs. Stationary Sensors. *AIChE J.* **1995**, *41*, 846−854.

(24) Rawlings, J. B.; Chien, I. L. Gage Control of Film and Sheet-Forming Processes. *AIChE J.* **1996**, *42*, 753−766.

(25) Heath, W. P. Orthogonal Functions for Cross Directional Control of Web Forming Processes. *Automatica* **1996**, *32*, 183−198.

(26) Rao, C. V.; Campbell, J. C.; Rawlings, J. B.; Wright, S. J. Efficient Implementation of Model Predictive Control for Sheet and Film Forming Processes. *Proceedings of the American Control Conference*, Albuquerque, NM, June 1997; pp 2940−2944.

(27) Rigopoulos, A.; Arkun, Y.; Kayihan, F. Model Predictive Control of CD Profiles in Sheet Forming Processes Using Full Profile Disturbance Models Identified by Adaptive PCA. *Proceedings of the American Control Conference*; Albuquerque, NM, June 1997; pp 1468−1472.

(28) Campbell, J. C.; Rawlings, J. B. Predictive Control of Sheet- and Film-Forming Processes. *AIChE J.* **1998**, *44*, 1713−1723.

(29) VanAntwerp, J. G.; Braatz, R. D. Fast Model Predictive Control of Sheet and Film Processes. *IEEE Trans. Control Sys. Technol.* **2000**, *8*, 408−417.

(30) Landlust, J.; Mesbah, A.; Wildenberg, J.; Kalbasenka, A. N.; Kramer, H. J. M.; Ludlage, J. H. A. An Industrial Model Predictive Control Architecture for Batch Crystallization. *Proceedings of the 17th International Symposium on Industrial Crystallization*, Maastricht, The Netherlands, Sep 14−17, 2008; pp 35−42.

(31) Daraoui, N.; Dufour, P.; Hammouri, H.; Hottot, A. Model Predictive Control During the Primary Drying Stage of Lyophilisation. *Control Eng. Pract.* **2010**, *18*, 483−494.

(32) Eaton, J. W.; Rawlings, J. B. Feedback Control of Chemical Processes Using On-Line Optimization Techniques. *Comput. Chem. Eng.* **1990**, *14*, 469−479.

(33) Chung, S. H.; Ma, D. L.; Braatz, R. D. Optimal Seeding in Batch Crystallization. *Can. J. Chem. Eng.* **1999**, *77*, 590−596.

(34) Biegler, L. T. Efficient Solution of Dynamic Optimization and NMPC Problems. In *Nonlinear Model Predictive Control*; Allgöwer, F., Zheng, A., Eds.; Springer: Basel, Switzerland, 2000; pp 219−243.

(35) Qin, S. J.; Badgwell, T. A. An Overview of Nonlinear Model Predictive Control Applications. In *Nonlinear Model Predictive Control*; Allgöwer, F., Zheng, A., Eds.; Springer: Basel, Switzerland, 2000; p 369−392.

(36) Binder, T.; Blank, L.; Bock, H.; Bulirsch, R.; Dahmen, W.; Diehl, M.; Kronseder, T.; Marquardt, W.; Schlöder, J. P.; Strykr, O. V. Introduction to Model Based Optimization of Chemical Processes on Moving Horizons. In *Online Optimization of Large Scale Systems*; Grötchel, M., Krumke, S. O., Rambau, J., Eds.; Springer: Berlin, 2001; pp 295−340.

(37) Sheikhzadeh, M.; Trifkovic, M.; Rohani, S. Real-Time Optimal Control of an Anti-Solvent Isothermal Semi-Batch Crystallization Process. *Chem. Eng. Sci.* **2007**, *63*, 829−839.

(38) Simon, L. L.; Nagy, Z. K.; Hungerbuhler, K. Model Based Control of a Liquid Swelling Constrained Batch Reactor Subject to Recipe Uncertainties. *Chem. Eng. J.* **2009**, *153*, 151−158.

(39) Mesbah, A.; Huesman, A. E. M.; Kramer, H. J. M.; Nagy, Z. K.; Van den Hof, P. M. J. Real-Time Control of a Semi-Industrial Fed-Batch Evaporative Crystallizer Using Different Direct Optimization Strategies. *AIChE J.* **2011**, *57*, 1557−1569.
(40) Mesbah, A.; Nagy, Z. K.; Huesman, A. E. M.; Kramer, H. J. M.; Van den Hof, P. M. J. Nonlinear Model-based Control of a Semi-industrial Batch Crystallizer using a Population Balance Modeling Framework. *IEEE Trans. Control Sys. Technol.* **2012**, *20*, 1188−1201.
(41) Julier, S. J.; Uhlmann, J. K. A New Extension of the Kalman Filter to Nonlinear Systems. *Proceedings of the 11th International Symposium on Aerospace/Defense Sensing, Simulation and Controls*, Orlando, FL, April 1997; pp 182−193.
(42) Julier, S. J.; Uhlmann, J. K. Unscented Filtering and Nonlinear Estimation. *Proc. IEEE* **2004**, *92*, 401−422.
(43) Romanenko, A.; Santos, L. O.; Afonso, P. A. Unscented Kalman Filtering of a Simulated pH System. *Ind. Eng. Chem. Res.* **2004**, *43*, 7531−7538.
(44) Schei, T. S. On-Line Estimation for Process Control and Optimization Applications. *J. Process Control* **2008**, *18*, 821−828.
(45) Hermanto, M. W.; Chiu, M. S.; Braatz, R. D. Nonlinear Model Predictive Control for the Polymorphic Transformation of L-Glutamic Acid Crystals. *AIChE J.* **2009**, *55*, 2631−2645.
(46) Mangold, M.; Buck, A.; Schenkendorf, R.; Steyer, C.; Voigt, A.; Sundmacher, K. Two State Estimators for the Barium Sulfate Precipitation in a Semi-Batch Reactor. *Chem. Eng. Sci.* **2009**, *64*, 646−660.
(47) Mesbah, A.; Huesman, A. E. M.; Kramer, H. J. M.; Van den Hof, P. M. J. A Comparison of Nonlinear Observers for Output Feedback Model-Based Control of Seeded Batch Crystallization Processes. *J. Process Control* **2011**, *21*, 652−666.
(48) Vrentas, J. S.; Vrentas, C. M. Drying of Solvent-Coated Polymer Films. *J. Polym. Sci., Part B: Polym. Phys.* **1994**, *32*, 187−194.
(49) Alsoy, S.; Duda, J. L. Drying of Solvent Coated Polymer Films. *Drying Technol.* **1998**, *16*, 15−44.
(50) Pakowski, Z.; Mujumdar, A. S. In *Handbook of Industrial Drying*; Mujumdar, A. S., Ed.; CRC Press: Boca Raton, FL, 2006; p 53−80.
(51) Price, P. E.; Wang, S.; Romdhane, I. H. Extracting Effective Diffusion Parameters from Drying Experiments. *AIChE J.* **1997**, *43*, 1925−1934.
(52) Fried, J. R. *Polymer Science & Technology*; Prentice Hall: Upper Saddle River, NJ, 2003.
(53) Brooker, D. B. Mathematical Model of the Psychrometric Chart. *Trans. ASABE* **1967**, *10*, 558−560.
(54) Leveque, R. J. *Finite Volume Methods for Hyperbolic Problems*; Cambridge University Press: Cambridge, U.K., 2002.
(55) Barttfeld, M.; Alleborn, N.; Durst, F. Dynamic Optimization of Multiple-Zone Air Impingement Drying Process. *Comput. Chem. Eng.* **2006**, *30*, 467−489.
(56) Dufour, P. Control Engineering in Drying Technology: Review and Trends. *Drying Technol.* **2006**, *24*, 889−904.
(57) Allanic, N.; Salagnac, P.; Glouannec, P. Optimal Constrained Control of an Infrared-Convective Drying of a Polymer Aqueous Solution. *Chem. Eng. Res. Des.* **2009**, *87*, 908−914.
(58) Price, P. E.; Cairncross, R. A. Optimization of Single-Zone Drying of Polymer Solution Coatings using Mathematical Modeling. *J. Appl. Polym. Sci.* **2000**, *78*, 149−165.
(59) Thomas, M. M.; Kardos, J. L.; Joseph, B. Shrinking Horizon Model Predictive Control Applied to Autoclave Curing of Composite Laminate Materials. *Proceedings of the American Control Conference*, Baltimore, MD, June 29−July 1, 1994; pp 505−510.
(60) Brosilow, C.; Joseph, B. *Techniques of Model-based Control*; Prentice Hall: Upper Saddle River, NJ, 2002.
(61) Diehl, M.; Ferreau, H. J.; Haverbeke, N. In *Nonlinear Model Predictive Control: Towards New Challenging Applications*; Magni, L., Raimondo, D. M., Allgöwer, F., Eds.; Springer: Berlin, 2009; pp 391−417.
(62) Biegler, L.; Cuthrell, J. Improved Infeasible Path Optimization for Sequential Modular Simulators II: The Optimization Algorithm. *Comput. Chem. Eng.* **1985**, *9*, 257−267.
(63) van der Merwe, R.; Wan, E. The Square-Root Unscented Kalman Filter for State and Parameter Estimation. *Proceedings of IEEE International Conference on Acoustics, Speech and Signal Processing*, Salt Lake City, UT, May 7−11, 2001; pp 3461−3464
(64) Rivera, D. E.; Morari, M.; Skogestad, S. Internal Model Control. 4. PID Controller Design. *Ind. Eng. Chem. Process Des. Dev.* **1986**, *25*, 252−265.
(65) Alsoy, S.; Duda, J. L. Modeling of Multilayer Drying of Polymer Films. *J. Polym. Sci., Part B: Polym. Phys.* **1999**, *16*, 1665−1674.